Modelling the Influence of Cardiac Motion on Electrical Excitation and the Magnetocardiogram

Stefan Fruhner[1,2], Harald Engel[1], Markus Bär[2]

[1]Technische Universität Berlin, Germany
[2]Physikalisch-Technische Bundesanstalt, Berlin, Germany

Abstract

Simulations of cardiac excitation were performed for cross sections of the human heart. To create computer models, magnetic resonance images (MRI) and magnetocardiograms (MCG) were acquired for a healthy human. The effect of geometry on properties of the magnetic field was investigated by running static simulations for two extreme cases – the relaxed state (diastole) and the contracted state (systole). The shape of the QRS complex and the T-wave substantially changes showing a weak QRS complex and elevated T-waves for the systolic geometry. In a second step we incorporated the dynamical aspect by implementing an interpolation algorithm to emulate cardiac contraction. The resulting simulated biosignals resembled the MCG showing a pronounced QRS complex as well as a T-wave of approx. the right amplitude. Hence, modelling cardiac excitation should also account for detailed geometry changes in order to quantiatively reproduce the shape of measured biosignals.

1. Introduction

The gain in computer power in recent years makes whole organ modelling a valuable application for investigating patient-specific computer models. Whereas simulations of the static electro-physiology of the heart have made big advances, the role of contraction often remains unrevealed. Earlier works by Keldermann, Nash and Panfilov [1] [2] already showed an influence of contraction on the excitation dynamics in reaction-diffusion systems. For example it was shown that mechanical deformations may lead to spiral breakup – one possible mechanism of the transition from ventricular tachycardia to fibrillation. Previous work [3] also revealed a dependency of geometry on computed biosignals and the need for taking cardiac contraction into account. In section 2 we briefly summarize our methods how this is realised. We also present our approach of creating appropriate finite element meshes. In section 3 we draw conclusions on the effect of motion on the MCG for two different ionic models.

2. Methods

2.1. Data acquisition and mesh generation

MCG time series were recorded for a couple of volunteers. These measurements were performed on a 83-SQUID machine at a sampling rate of $1kHz$ in a magnetically shielded room. Directly afterwards magnetic resonance images were acquired. This was done using a time-resolved tagged MRI protocol on a $1.5T$ machine. Using the R-wave in the *electrocardiogram* (ECG) as trigger 17 images were recorded with a time step of $32ms$ covering a complete contraction cycle. The original MR images have a resolution of 256×256 pixels. One pixel has an edge length of $1480\mu m$ (cf. fig. 1). A segmentation was done manually using the software package ITK-SNAP [1]. For the dataset of a 35 year old healthy male a person-specific finite element mesh was constructed. The regions of interest – cardiac regions and the ventricles – were extracted. In the next step the borders of these regions were estimated and smoothed using a third-order B-Spline algorithm. Feeding the boundaries into the software package *triangle* [2] two dimensional finite element meshes were created. For cardiac regions an averaged edge length of $250\mu m$ was chosen. So the resulting area constraint for one triangle was set to $31250\mu m^2$. For extra-cardiac regions and the cavities this area constraint was reduced by the factor 0.5. In the following step three-dimensional meshes were constructed by creating a second layer in $250\mu m$ distance in the third spatial dimension. The tetrahedralisation was done using *tetgen* [3]. The resulting meshes meet strict conditions concerning the angle and volume distributions.

2.2. Simulation details

The cardiac excitation is modelled using the *bidomain equations* – a set of partial differential equations for the extracellular potential Φ_e and the transmembrane potential V_m, which is defined as the difference of intra- and extra-

[1]http://www.itksnap.org
[2]http://www.cs.cmu.edu/ quake/triangle.html
[3]http://tetgen.berlios.de

cellular potentials $V_m = \Phi_e - \Phi_i$:

$$\nabla \cdot \left(\underline{\underline{\sigma}}_i \nabla V_m \right) = -\nabla \cdot \left(\left(\underline{\underline{\sigma}}_i + \underline{\underline{\sigma}}_e \right) \right) \nabla \phi_e \,, \tag{1}$$

$$\nabla \cdot \left(\underline{\underline{\sigma}}_i \nabla V_m \right) + \nabla \cdot \left(\underline{\underline{\sigma}}_i \nabla \phi_e \right) = \beta \left(C_m \frac{\partial V_m}{\partial t} + I_{Ion} \right), \tag{2}$$

where β is the dimensionless surface-to-volume ratio and C_m is the membrane capacitance [4] [5]. The parameters describing the conduction tensor $\underline{\underline{\sigma}}_{i,e}$ are chosen accordingly to [6] as $\sigma_{il} = 0.174 S/m, \sigma_{it} = 0.019 S/m, \sigma_{el} = 0.625 S/m, \sigma_{et} = 0.236 S/m, \sigma_o = 1 S/m$. The indices l and t represent longitudinal and transversal conductivity orientations. The ionic models enter via the ion currents I_{Ion}. In this work two of them were applied to the simulations: a 4-variable minimal model by Bueno-Orovio, Cherry and Fenton (BCF) [7] and a 14-variable model by ten Tusscher (TNNP) [8]. Each of these models is tuned to fit the ionic dynamics to epi-, myo- and endocardial cells.

2.3. Cardiac motion

The bidomain solver only handles static simulation meshes. To introduce cardiac motion taken from time-resolved MRI a sophisticated interpolation algorithm was implemented. Simulations of the static heart are performed using different finite element meshes that belong to different times of the cardiac cycle. After one simulation step of $32ms$ length the ionic state variables and potential values are saved. Interpolated values are computed for all nodes of the following mesh by mapping all nodes of the new mesh onto the coordinate system of the preceding mesh. This is done using deformation vectors that are estimated for every node. The next step is to find the surrounding tetrahedron for every node of the new mesh and to compute its *barycentric coordinates*. They are used to complete the interpolation. To estimate the deformation vectors we use the fact that a set of points – referred to as *control points* – in the raw images are tagged, so that their trajectories can be recorded. Using a similar interpolation technique as described above, the trajectories of *each* node can be calculated. The accuracy of these trajectories is limited by the density of control points. We apply 81 control points equally distributed over the cardiac region (cf. figure 1).

The interpolation can only be computed for such nodes of the new mesh which are enclosed by a tetrahedron whose edge points are based on the same ionic model. Otherwise an interpolation becomes impossible because different models can have different numbers of state variables. So in regions where nodes with different cellular properties (e.g. epi-, endo- or myocardial) are close to each other alternative methods of interpolation are yet to be developed. So far it turned out to be problematic to use the closest valid tetrahedron for interpolation since this may lead to stimulation of regions and further spreading of an excitation wave that has not existed before. Therefore we decided to set the state values of such a node to those of the closest node utilising the same ionic model. This method guarantees consistent interpolation results but lacks of accuracy and leads to discontinuities in the calculated time series of the ECG or the MCG.

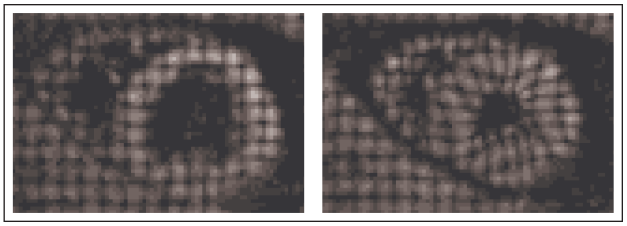

Figure 1. Tagged magnetic resonance images for diastolic (left) and systolic (right) heart geometry. Horizontally and vertically tagged images were combined to visualise the control points (black). From the locations of these points in different images trajectories can be recorded. The shown image sizes correspond to $11.9cm \times 8.2cm$.

2.4. Region allocation and fibre orientation

To account for different electrical properties of cardiac cells depending on their location within the tissue, we use three different sets of parameters for epi-, endo- and myocardial tissue for both ionic models. Generally myocardial cells exhibit a longer action potential as their epi- and endocardial neighbours. The property 'cell type' has to be assigned to every node in the finite element meshes. For each node the distances to the epi- and endocardial borders are computed. The connection between these two points at the inner and the outer boundary defines a line. Depending on the node's position on that line the label 'endocardial' is chosen, if it is more than 75% of the length away from the epicardial boundary. The epicardial range is chosen to be 0 - 25% of the line. All other cases are labelled as myocardial.

The elongated shape of cardiac cells results in a strong anisotropy in electrical conductivity. Since the fibre orientation cannot be taken from MR images, it has to be assigned artificially. According to Streeter [9] the fibre orientation is set to rotate linearly from an angle of -45° to $+70^\circ$ (with respect to the out-of-plane direction in fig. 2) from the epicardial to the endocardial boundary. The in-plane orientation is chosen to be perpendicular to the line connecting the closest epicardial and the closest endocardial boundary point.

2.5. Stimulation protocol

The cross sections of the heart do not include a natural stimulation region as the sinus node, where in the heart the stimulus is emitted periodically. It is located in the right

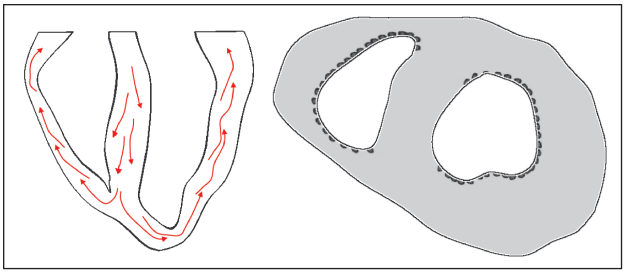

Figure 2. **L:** Vertical cross section of human cardiac ventricles. The arrows denote the spreading of the excitation through the heart (schematic). **R:** Horizontal cross section of the heart viewed from below (model, diastolic state). Shown is the transmembrane potential $1.74ms$ after stimulation. Highlighted in dark grey are the regions of high potential that contain the stimulation points.

atrium which is electrically separated from the ventricles. The atrioventricular node directly couples the stimulus into the HIS bundle and the Purkinje fibre system. It guides the excitation along the septum in the direction of the apex (cf. fig. 2 (left)). From there the excitation spreads upwards along the inner wall of the ventricles.

To mimic this situation a set of stimulation points along the inner walls of the ventricles was chosen, where the transmembrane current was set to $50\mu A/\mu m^2$ for a duration of $1ms$. Figure 2 (right) exemplifies the stimulation region for one simulation mesh.

2.6. Magnetic field

The magnatic fields are computed by the forward-method, solving the *Biot-Savart* integral:

$$\mathbf{B}(\mathbf{r}) = \frac{\mu_0}{4\pi} \int_{\mathrm{V}} \mathbf{j}(\mathbf{r}') \times \frac{\mathbf{r} - \mathbf{r}'}{|\mathbf{r} - \mathbf{r}'|^3} \, \mathrm{dV}' \,. \qquad (3)$$

The *net currents* $\mathbf{j}(\mathbf{r}')$ of the extra- and intracellular domains act as sources of the magnetic field and are computed as gradients of the electrical potentials. The magnetic field is calculated for a location in front of the body's surface which corresponds to the setting in the experiments. The distance is selected such that the shape of measured $\mathbf{B}$-fields as well as the amplitude of the QRS-complex and the T-wave are remodelled as best as possible.

3. Results

We ran simulations for the two different ionic models – BCF and TNNP – in static simulation setup for a diastolic and a systolic geometry. The dynamic simulation is started using the diastolic mesh geometry. The stimulation is always initiated at $t = 0$.

Figure 3 shows a measured MCG that belongs to the proband whose MR images were used to create the FE meshes. The ratio of the amplitude of the R-wave and the T-wave amplitude (*RT ratio*) is approximately 3.2.

To find MCG signals resembling these measured data we computed the magnetic field for several distances to the outer boundary of the left ventricle in front of the chest. In the distance interval $[5.0cm, 7.0cm]$ we could verify that a positive T-wave can be observed in B_z. For simulations in diastolic mesh geometry the R-wave amplitude is larger than the T-wave amplitude. Within the interval there is a clear dependence of the T-wave amplitude on the distance: For the diastolic geometry the maximum value increases about $10pT$ for the BCF model. For the systolic geometry the effect is smaller. The maximum value of the QRS-complex decays for increasing distance. In other words, the RT ratio varies with the distance.To draw comparisons we have chosen the distance to be $7cm$, where the shape of the MCG resembles best that one of the experimental curve shown in fig. 3. These simulation results are shown in fig. 4.

For static simulations we find large differences in the shape of the curves. In the diastolic case the maximum of the T-wave has a by $13pT$ smaller value for the minimal model as for the systolic case. It is also shifted to arise $8ms$ earlier using the systolic geometry. For the TNNP model both differences are larger ($16pT$ for the maximum, $16ms$ for the shift). The QRS complex disappears almost completely for both models in systolic geometry.

The gap between all these differences can be filled using the dynamical approach. The T-wave is observed in time and amplitude in between the extreme cases of diastolic or systolic geometry. As expected, the dynamic simulation protocol reproduces the QRS complex of the diastolic case completely, because exactly the same simulation mesh was used in both cases. The RT ratio is 3.8 and 2.5 for the BCF and the TNNP model. Both values describe the experimental curve much better than the values of the static simulations (cf. table 1).

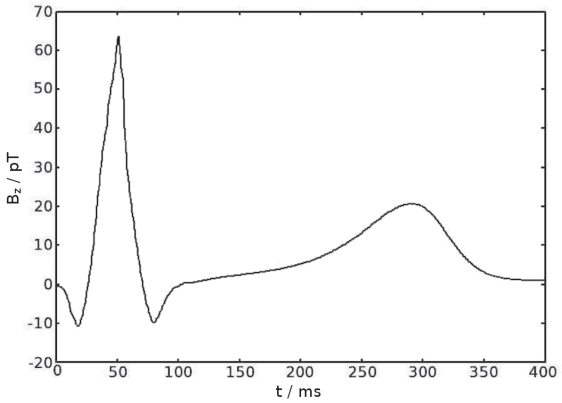

Figure 3. Averaged measured MCG in central channel [3]

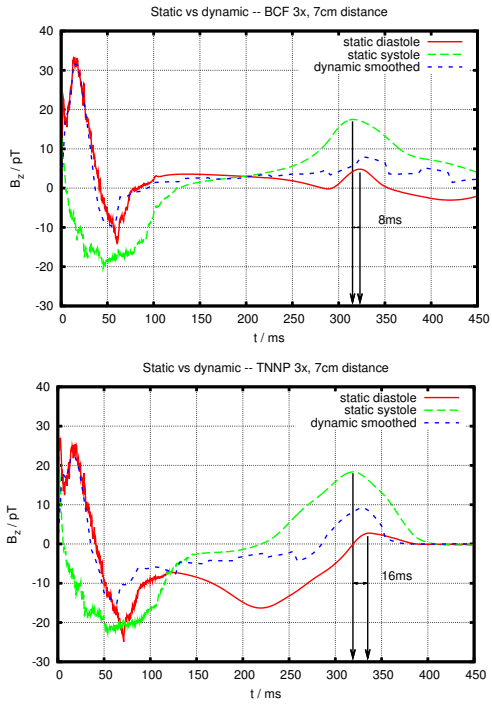

Figure 4. Magnetic fields B_z for static and dynamic simulations in $7cm$ distance to the active surface of the left ventricle, **top**: BCF model, **bottom**: TNNP model

4. Discussion and conclusions

In comparison to previous work [3] the differences in the MCGs for the two extreme geometries are more pronounced. One reason is that here both ventricles are modelled – not only the left one as in [3] . This results in larger differences in geometry that affect the biosignals more strongly. In the present work the QRS complex even disappears for the systolic geometry. On the other hand the T-wave shows a much more pronounced peak compared to the one in the experiments.

In the heart the QRS complex occurs at the start of contraction, whereas the T-wave occurs during relaxation. This is represented by the static simulations: With the relaxed mesh the T-wave is suppressed while it is overrated for the contracted mesh. Vice versa the QRS complex is formed using the relaxed mesh but not for the other case. Only the dynamic simulations contain information of both – the systole and the diastole – in the MCG. The inclusion of cardiac motion results in the MCG signal to develop a QRS peak as well as an appropriate T-wave. The ratio of their maxima is similar to the value from the experiments. The method of interpolation still needs to be improved. The approach also offers the opportunity to calculate the mechanical stresses during cardiac contraction from experimental data without using detailed models on calcium dynamics and stress-activated channels in cardiac myocytes.

simulation setting	RT ratio BCF	RT ratio TNNP
static diastole	6.6	8.3
static systole	-	-
dynamic	3.8	2.5

Table 1. Ratio of R-wave amplitude to T-wave amplitude (*RT ratio*) for the different simulation settings

Acknowledgements

The software *CARP* (Cardiac Arrhythmia Research Package) that was used to solve the bidomain equations was written by G. Plank and E.J. Vigmond. The magnetic resonance images were acquired at the DHZ Berlin (Deutsches Herzzentrum) which was possible due to a cooperation with B. Schnackenburg, I. Paetsch and E. Fleck. We would also like to thank H. Koch and S. Bauer for valuable discussions and software engineering.

References

[1] Keldermann RH, Nash MP, Panfilov AV. Pacemakers in a reaction-diffusion mechanics system. J Stat Phys 07 2007; Vol. 128(1/2):375–392.

[2] Panfilov AV, Keldermann RH, Nash MP. Drift and breakup of spiral waves in reaction-diffusion-mechanics systems. Proc Natl Acad Sci USA 2007;104(19):7922–7926.

[3] Bauer S, Weber dos Santos R, Schmal T, Nagel E, Bär M, Koch H. QRS width and QT time alteration due to geometry change in modelled human cardiac magnetograms. CinC 2005;32:639–642.

[4] Vigmond E, Weber dos Santos R, Prassl A, Deo M, Plank G. Solvers for the cardiac bidomain equations. Prog Biophys Mol Biol 2008;96(1-3):3 – 18.

[5] Bauer S, Röder G, Bär M. Alternans and the influence of ionic channel modifications: Cardiac three-dimensional simulations and one-dimensional numerical bifurcation analysis. Chaos 2007;17:015104.

[6] Plank G, Leon L, Kimber S, Vigmond E. Defibrillation depends on conductivity fluctuations and the degree of disorganization in reentry patterns. J Cardiovasc Electrophysiol Feb. 2005;16(2):205–16.

[7] Bueno-Orovio A, Cherry EM, Fenton FH. Minimal model for human ventricular action potentials in tissue. J Theor Biol 2008;253(3):544 – 560.

[8] ten Tusscher KHWJ, Noble D, Noble PJ, Panfilov AV. A model for human ventricular tissue. Am J Physiol Heart Circ Physiol 2004;286:H1573–H1589.

[9] Streeter DDJ. Gross morphology and fiber geometry of the heart. Handbook of Physiology 1979;1:61–112.

Address for correspondence:

Technische Universität Berlin, ITP
EW 7-1 Stefan Fruhner
Hardenbergstraße 36,10623 Berlin, Germany
stefan.fruhner@tu-berlin.de